Embedment Behavior of Low-to-Medium Diameter Bolts in Douglas-Fir Glued Laminated Timber

Zheng Li,[a,*] Chao Yang,[b] Zhiqiang Qin,[c] and Lichao Wei [c]

Reliable embedment properties are essential for the design of bolted glulam connections, yet most available equations were developed for sawn timber. This study investigated the embedment behavior of Douglas-fir glued-laminated timber by full-hole tests on 13 specimen series with a constant 1 mm hole clearance. The matrix was designed to isolate the effects of bolt diameter (8 to 16 mm), load-to-grain angle (0 to 90°), and member thickness (30 to 40 mm). Increasing bolt diameter markedly increased embedment stiffness, from 4.20 to 8.46 kN/mm in the 35 mm parallel-to-grain series, while strength changed only slightly. For the 12 mm reference series, both yield strength and stiffness decreased from 0° to 60° and then partially recovered at 90°, confirming pronounced anisotropic behavior. Increasing thickness improved the overall response, although the strength trend over 30–35–40 mm was not strictly monotonic. Existing Eurocode 5 and NDS equations showed noticeable deviations, especially for off-axis loading. A modified Hankinson-type model gave the closest agreement with the measured yield embedment strengths and offers a more reliable basis for the design and assessment of low-to-medium diameter bolted glulam connections.

DOI: 10.15376/biores.21.3.6781-6800

Keywords: Glued laminated timber; Embedment strength; Low-to-medium diameter bolts; Load-to-grain angle; Prediction model

*Contact information: a: College of Material Science and Engineering, Northeast Forestry University, Harbin 150040, China; b: College of Mechanical and Electrical Engineering, Northeast Forestry University, Harbin 150040, China; c: School of Civil Engineering and Transportation, Northeast Forestry University, Harbin 150040, China; *Corresponding author: zli6073@163.com*

INTRODUCTION

Glued laminated timber (glulam) has become a mainstream engineered wood product for long-span and mid-rise timber construction because it combines good dimensional stability with efficient use of lumber resources (Issa and Kmeid 2005; Tuhkanen *et al.* 2018). The safety and ductility of glulam structures depend strongly on their joints, and dowel-type fasteners remain the most common load-transfer mechanism in practical beam-to-column and splice connections (Smith *et al.* 2002; Ottenhaus *et al.* 2021). Within the European Yield Model, the embedment strength of the timber member is one of the governing input parameters for connection resistance (Johansen 1949).

Most classical embedment studies were developed for solid sawn timber rather than laminated products. Early work established the relevance of fastener diameter and loading direction (Hager 1930; Mack 1981). More recent studies clarified the influence of density, loading angle, and testing protocol (Sandhaas *et al.* 2013; Cabrera *et al.* 2022; Aquino *et al.* 2024). In parallel, methodological comparisons showed that half-hole and full-hole arrangements may yield comparable average embedment strengths, but they can generate

different confinement conditions and different failure manifestations, which complicates cross-study comparison (Santos *et al.* 2010; Ottenhaus *et al.* 2022; Wang *et al.* 2025).

For engineered wood products, direct transfer of sawn-timber equations is not always reliable. Tuhkanen *et al*. (2018) reported that the number of layers affects embedment behavior in glulam. Schweigler *et al.* (2016) demonstrated a strong load-to-grain-angle dependence in laminated veneer lumber. Xu *et al.* (2021) showed that fastener type affects parallel-to-grain embedment response in glulam, and Xu *et al.* (2022) reported distinct behavior for fully threaded bolts in glulam. Jeong *et al.* (2018) further demonstrated that the bearing properties of glulam vary with material orientation. These studies indicate that lamination, product architecture, and fastener geometry should be treated explicitly when formulating design-oriented embedment models.

Beyond the difference between sawn timber and glulam in average embedment strength, the failure mechanism of dowel-type timber connections is also strongly affected by the layered architecture and stress redistribution capacity of the member. A desirable ductile response is usually associated with timber embedment and yielding of the steel dowel; however, brittle failure modes such as splitting, row shear, plug or block shear, net-tension failure, and edge- or end-related fracture may occur when local tensile or shear stresses around the fastener exceed the corresponding resistance of the timber member (Cabrero *et al.* 2019; Ottenhaus *et al.* 2021; Yurrita *et al.* 2021). These brittle modes are especially relevant for engineered timber products because lamination, glue-line arrangement, local material heterogeneity, and member geometry can alter the stress path around the bolt hole and affect crack initiation and propagation. Previous studies have also shown that the number of layers, fastener type, loading direction, and test configuration can noticeably change the measured embedment response of glulam and other laminated products (Tuhkanen *et al.* 2018; Ottenhaus *et al.* 2022; Xu *et al.* 2022). Therefore, the behavior of bolted glulam connections should not be interpreted only through equations calibrated for solid sawn timber, but should also be examined in relation to the failure modes and material architecture specific to glulam.

Anisotropy is a central feature of glulam embedment behavior. Although glulam is manufactured from graded laminations and has improved dimensional stability compared with solid timber, each lamella still retains the orthotropic characteristics of wood. Consequently, the local response near a dowel-type fastener depends on the relationship between the loading direction and the longitudinal, radial, and tangential material directions. In general, timber exhibits much higher resistance and stiffness parallel to the grain than perpendicular to the grain, whereas tensile stresses perpendicular to the grain can promote splitting and brittle crack propagation. For glulam, this directional dependence is further influenced by lamination layout, growth-ring orientation, glue lines, and local stress redistribution between adjacent laminations. Jeong *et al.* (2018) showed that the bearing properties of oriented glulam vary markedly with material orientation, while Schweigler *et al.* (2016) reported a pronounced load-to-grain angle dependence in laminated veneer lumber. These findings provide the physical basis for using an angle-dependent Hankinson-type formulation when predicting the embedment response of laminated timber products.

A second gap concerns the structure of available experimental programs. Many studies address one or two variables at a time, often with large-diameter fasteners or changing hole-clearance conditions. For low-to-medium diameter bolts in Douglas-fir glulam, published data remain limited, especially when a fixed 1 mm hole clearance is maintained. Moreover, discussions sometimes generalize angle or thickness effects beyond

the subset actually tested. To avoid that ambiguity, the present paper makes the scope of each comparison explicit.

To address these gaps, this study conducted a systematic experimental investigation on the embedment strength of glulam under dowel-type fastener loading. A total of 13 test groups were designed to evaluate the effects of four key parameters: fastener diameter (M8, M10, M12, M16), loading-to-grain, specimen thickness (30 mm, 35 mm, 40 mm), and glulam grain orientation. All specimens featured a consistent hole-to-fastener clearance of 1 mm, reflecting practical construction practices. Based on the anisotropic and layered nature of glued laminated timber, this study was guided by three testable hypotheses. First, under a fixed 1 mm hole clearance, bolt diameter was expected to have a stronger influence on embedment stiffness than on normalized embedment strength because a larger projected bearing area mobilizes a greater volume of wood while also increasing local stress concentration near the hole edge. Second, load-to-grain angle was expected to govern both embedment strength and failure mode according to a Hankinson-type anisotropic relationship, with oblique loading producing combined compression, shear, and transverse tensile stresses. Third, member thickness was expected to affect stiffness and deformation stability by changing the volume of wood participating in stress dispersion around the bolt hole. These hypotheses were examined using 13 full-hole embedment series with controlled bolt diameter, load-to-grain angle, member thickness, and hole clearance.

EXPERIMENTAL

Materials

The glulam used in this experiment was made from Douglas fir and was supplied by Nantong Jiazhu Construction Co., Ltd. The material properties were evaluated using standardized experimental testing methods that adhered to Chinese national standards (GB/T 50329 2012; GB/T 26899 2022). Before specimen fabrication, the boards were visually inspected, and regions containing visible knots, checks, resin pockets, local delamination, or glue-line defects near the intended embedment zone were avoided. The test specimens were cut so that the bolt hole was located away from visible manufacturing defects and edge discontinuities. The available quality-control information indicated that the material satisfied the requirements for structural glulam; however, detailed batch-level records for adhesive formulation, pressing pressure, and curing conditions were not fully available. This has now been stated as a limitation, because glue-line quality, lamination defects, and manufacturing variability may contribute to the scatter in embedment strength and stiffness. The mean elastic modulus of the glulam was 12,850 MPa. The compressive strength and tensile strength were 48.2 MPa and 15.6 MPa, respectively. The shear strength was 8.3 MPa. The average density of the material was 466 kg/m^3, with a coefficient of variation (COV) of 2.6%, indicating relatively low variability in density among test samples. All material property tests were conducted under ambient temperature conditions, with the wood specimens maintained at a consistent moisture content of 12%. The measured material properties are summarized in Table 1. The bolts were grade 12.9, with a yield strength of 1,080 MPa and a tensile strength of 1,200 MPa. High-strength bolts were selected to minimise bolt bending and to concentrate the response on timber embedment. The bolts were partially threaded, but the embedment zone was positioned along the smooth shank in all test configurations so that thread-bearing effects were intentionally excluded.

Table 1. Material Properties of Glulam

Properties	Values (COV)
Modulus of elasticity (MPa)	12850 (1.4%)
Compressive strength (MPa)	48.2 (2.56%)
Tensile strength (MPa)	15.6 (7.6%)
Shear strength (MPa)	8.3 (6.7%)
Density (kg/m3)	466 (2.6%)

Specimen Preparation

Two embedment test arrangements are widely used in the literature: the half-hole (HH) test and the full-hole (FH) test. Previous comparisons have shown that the two methods can deliver similar mean embedment strengths, but the associated boundary conditions and local damage patterns are not identical (Hirai 1989; Sawata *et al.* 2002; Santos *et al.* 2010; Franke *et al.* 2014; Ottenhaus *et al.* 2022). Because the present work aimed to study practical bolt-in-hole behavior under combined changes of diameter, angle, and thickness, the FH configuration was adopted.

A total of thirteen specimen series were prepared, with eight replicates per series. Four nominal bolt diameters were considered (M8, M10, M12, and M16). The drilled hole diameter was fixed at d + 1 mm for all specimens. This clearance was intentionally controlled rather than treated as an independent variable. The purpose was to eliminate clearance-induced variability and to approximate the practical tolerance commonly encountered in bolted glulam joints. Hole clearance can affect initial slip, the onset of local contact, stress redistribution, and the measured initial stiffness. Therefore, the present conclusions should be interpreted for connections with similar clearance conditions. A dedicated clearance matrix would be required to quantify the independent influence of smaller or larger hole tolerances. The matrix included one dedicated diameter subset, one reference angle subset, and two parallel-to-grain thickness subsets. All geometric parameters satisfied (ASTM D 5764 2018). The specific parameters are detailed in Table 2, and schematic diagrams of each parameter configuration are shown in Fig. 1. Using GL35-8-0 as an example, here is the meaning of specimen numbering: In this designation, 'GL' stands for glulam; '35' indicates that the specimen is 35 mm thick; '8' denotes that the specimen is 8 mm in diameter; and '0' signifies that the load-to- grain angle is 0°.

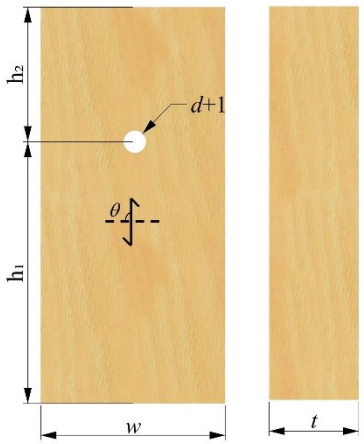


Fig. 1. Schematic diagram of the embedment test specimen

Table 2. Geometry and Details of the Tested Specimen

Specimen code	*d* (mm)	*w* (mm)	*t* (mm)	h_1 (mm)	h_2 (mm)	θ (°)	Number of replicates
GL35-8-0	8	90	35	84	84	0	8
GL35-10-0	10	90	35	84	84	0	8
GL35-12-0	12	90	35	84	84	0	8
GL35-16-0	16	90	35	84	84	0	8
GL30-12-0	12	90	30	84	84	0	8
GL30-12-30	12	90	30	84	84	30	8
GL30-12-45	12	90	30	84	84	45	8
GL30-12-60	12	90	30	84	84	60	8
GL30-12-90	12	90	30	84	84	90	8
GL30-16-0	16	90	30	84	84	0	8
GL30-16-90	16	90	30	84	84	90	8
GL40-12-0	12	90	40	84	84	0	8
GL40-16-0	16	90	40	84	84	0	8

Notes: *d* = nominal bolt diameter; *w* = width of test specimen; h_1= loaded length; h_2 = unloaded length; θ = load-to-grain

Test Setup

The configuration and measurement of the full-hole embedment test are illustrated in Fig. 2. The experimental procedure involved the implementation of continuous displacement control, whereby a constant loading rate of 1 mm/min was applied (ASTM D 5764 2018). The test was terminated when the embedment depth reached half the fastener diameter, or when the maximum load was attained and began to decrease. The load data were acquired using a load transducer. The displacement of the loading head was measured with two displacement transducers, which were securely mounted on the testing machine frame. The measurements from both transducers were then averaged to ensure greater accuracy. It is important to highlight that a deliberate clearance has been engineered between the loading device and the glulam. This intentional gap is designed to prevent any type of frictional contact from occurring between the two components during their operational interaction.

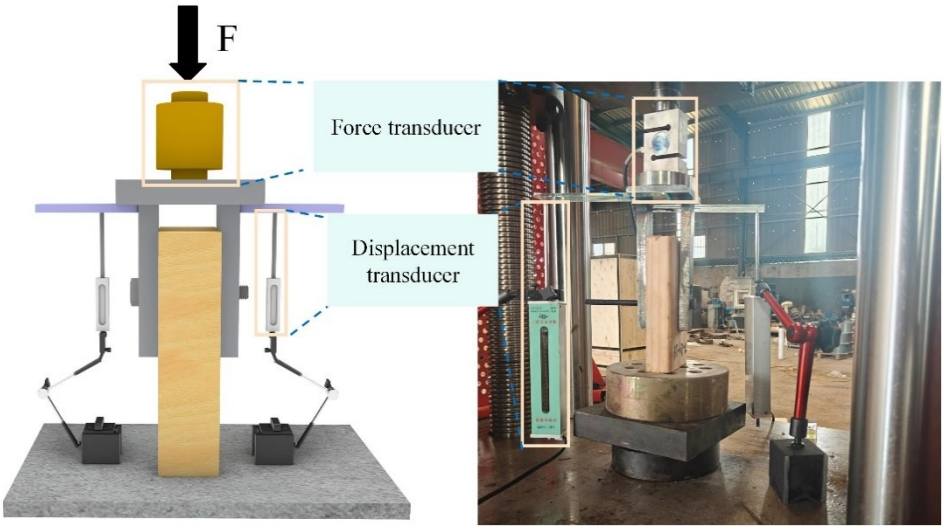


Fig. 2. Full-hole embedment test setup and instrumentation

The 5% offset method, as outlined in (ASTM D 5764 2018), is advocated for the delineation of the yield load, as shown in Fig. 3. First, the initial slope line was offset by 5% in the direction of the dowel diameter. Subsequently, the load value corresponding to the intersection point of the aforementioned offset line and the load-displacement curve was determined. The yield load was thus provided. In the event that the load value at this intersection exceeded the displacement value corresponding to the maximum load, the maximum load value was designated as the yield load. The embedment strength is calculated as shown in Eqs. 1 and 2,

$$f_{h,y} = \frac{F_y}{d \cdot t} \quad (1)$$

$$f_{h,u} = \frac{F_{max}}{d \cdot t} \quad (2)$$

where $f_{h,y}$ and $f_{h,u}$ are the yield embedment strength and ultimate embedment strength, F_y and F_{max} are the yield load and ultimate load taken by 5% offset method. The embedment stiffness K_i is defined according to (EN 383 2007) as the slope of the straight line connecting the load points 0.1 F_{max} and 0.4 F_{max}.

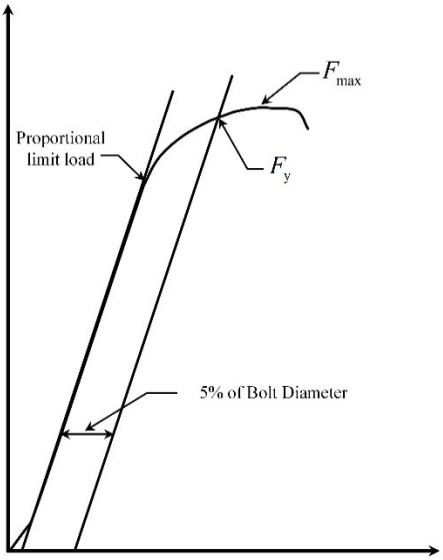


Fig. 3. Properties determined from 5% offset method (ASTM D 5764 2018)

RESULTS AND DISCUSSION

Failure Modes

The failure modes observed in embedment specimens exhibit distinctive characteristics that are significantly impacted by the test parameters, particularly the loading direction (specifically the grain angle) and the fastener diameter. As shown in Fig. 4, three representative failure modes were identified across all test groups, the occurrence of which is directly related to the interplay between these critical variables.

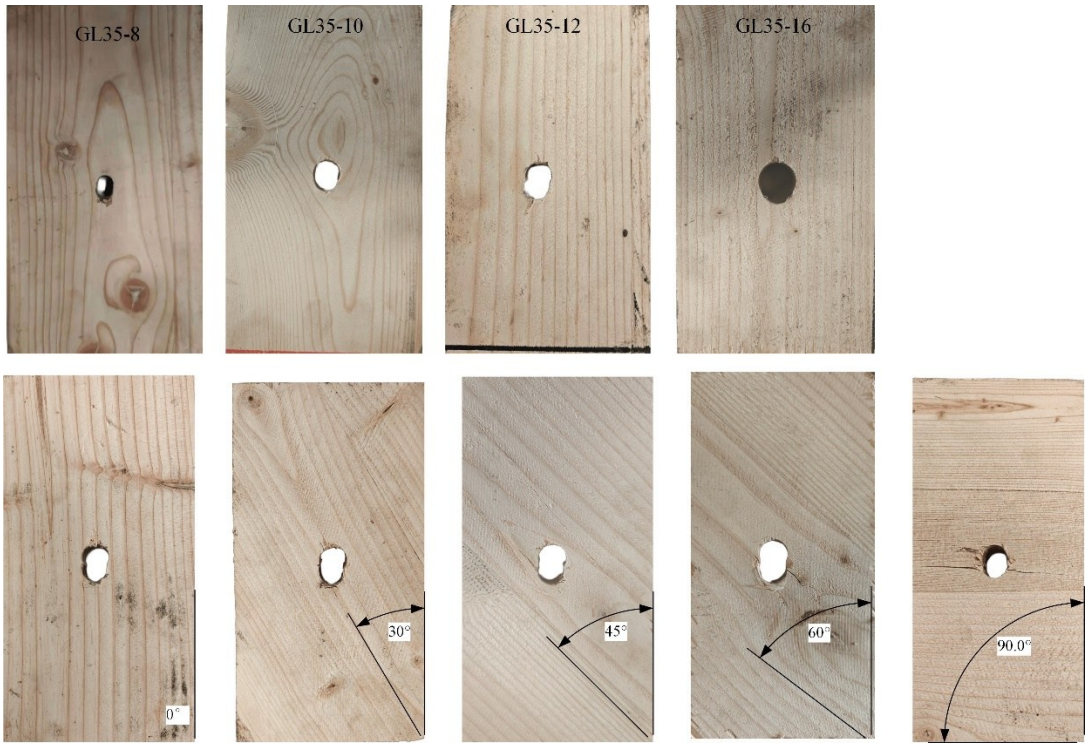


Fig. 4. Typical failure mode of specimens

The observed failure modes can be interpreted from the anisotropic stress-transfer mechanism around the bolt hole. Under parallel-to-grain loading, the bearing pressure is mainly resisted by longitudinal compression of wood fibers, and the high longitudinal compressive capacity allows local crushing and fiber bending to develop before unstable splitting occurs. The contact stress is not uniformly distributed over the projected bearing area; instead, it concentrates near the loaded edge of the hole, where local fiber buckling, crushing, and longitudinal crack initiation are most likely to occur. As the load-to-grain angle increases, the contact force can be decomposed into longitudinal compressive and transverse tensile/shear components. Because the tensile strength perpendicular to grain and the rolling-shear resistance of wood are much lower than longitudinal compression capacity, oblique loading promotes crack propagation along the grain and, in some cases, along or near lamination interfaces. This explains why the 45° and 60° specimens showed denser and longer splitting cracks, whereas the 0° specimens mainly exhibited localized crushing and fiber bending. Larger bolt diameters enlarged the contact region but also increased the stress gradient and the extent of local crushing, which is consistent with the wider compression zones observed around M16 bolts. As the loading-grain angle increases, the tensile stress component acting across the wood cross-section (the primary factor inducing splitting failure) also increases. Concurrently, the compressive stress component along the wood axis (which primarily induces fiber bending deformation) concomitantly weakens.

Mean Load-Displacement Response

As shown in Fig. 5, the mean load-displacement curves were derived for all 13 test groups. Each of these curves exhibits three phases that are distinctly recognizable: an initial linear elastic phase, followed by a yield phase, and concluding with a post-peak phase. The mean load-displacement curve for all specimens did not demonstrate a discernible

descending phase, as the test protocol stipulated the cessation of loading based on the bolt attaining a predetermined depth of embedment within the wood. Nevertheless, subtle variations can be observed in the post-yield mechanical responses among the different groups. Notably, when the load was applied at 0° (*i.e.*, aligned with the wood grain), all specimens displayed a classic ideal plastic behavior in their load-displacement profiles. In contrast, specimens subjected to loading at non-zero angles (*i.e.*, not aligned with the grain direction) exhibited a certain degree of strain hardening after reaching the yield point, which was eventually followed by a reduction in load-bearing capacity. This observed mechanical behavior has been previously reported and documented in the relevant literature (Xu *et al.* 2024).

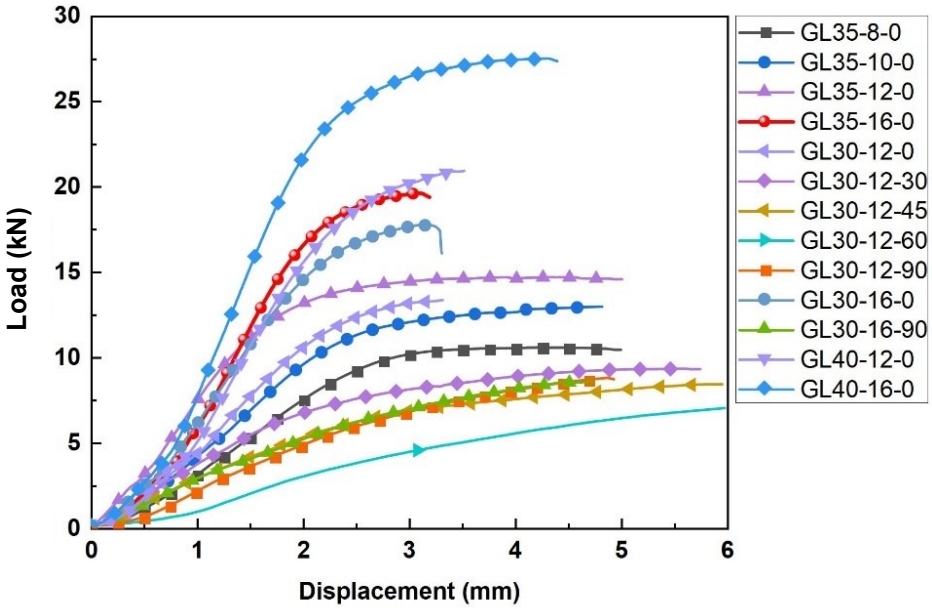


Fig. 5. The average embedment load-displacement curves

Summary of Test Results

The experimental results are summarized in Table 3, which reports the average values of the embedment characteristics for each series of specimens, along with their corresponding COV. With the exception of the GL30-12-60 group, where relatively high variability was observed due to factors associated with testing angle, the coefficients of variation for all other specimen groups remained within acceptable ranges. Furthermore, the data from all series demonstrated a high degree of similarity.

Table 3. Summary of Test Results

Specimen code	$f_{h,y}$ (MPa)	COV (%)	SD (MPa)	$f_{h,u}$ (MPa)	COV (%)	SD (MPa)	K_i (kN/mm)	COV (%)	SD (kN/mm)
GL35-8-0	36.9	6.0	2.214	38.5	3.6	1.386	4.2	7.5	0.315
GL35-10-0	34.66	11.8	4.090	36.0	7.9	2.844	5.05	12.0	0.606
GL35-12-0	33.3	2.6	0.866	35.4	6.2	2.195	7.4	8.9	0.659
GL35-16-0	34.48	8.1	2.793	35.9	9.6	3.446	8.46	16.4	1.387
GL30-12-0	35.9	4.2	1.508	37.7	3.8	1.433	5.8	5.9	0.342
GL30-12-30	21.6	6.7	1.447	25.9	6.9	1.787	4.0	7.3	0.292
GL30-12-45	18.7	17.2	3.216	24	17.7	4.248	3.0	10.2	0.306
GL30-12-60	17.4	32.3	5.620	24.0	37.3	8.952	2.4	31.3	0.751
GL30-12-90	21.8	25.1	5.472	26.9	22.8	6.133	3.3	21.0	0.693
GL30-16-0	34.8	6.2	2.158	37.1	6.0	2.226	7.6	14.9	1.132
GL30-16-90	15.9	7.5	1.192	18.6	8.7	1.618	2.88	6.7	0.193
GL40-12-0	41.3	3.9	1.611	42.6	4.3	1.832	7.36	16.1	1.185
GL40-16-0	41.48	7.8	3.235	42.9	6.7	2.874	11.3	10.3	1.164

Statistical Analysis

Statistical analysis was performed to validate the effects of bolt diameter, load-to-grain angle, and member thickness on the measured embedment properties. The yield embedment strength, ultimate embedment strength, and embedment stiffness were analyzed for the corresponding controlled specimen subsets. One-way analysis of variance (ANOVA) was used to compare different parameter levels, and a significance level of $p<0.05$ was adopted. The effect size was expressed using eta-squared (η^2). This analysis was intended to distinguish statistically supported parameter effects from descriptive trends observed in the mean values. The statistical results showed that bolt diameter had no significant effect on yield or ultimate embedment strength within the tested range, whereas its effect on embedment stiffness was significant. The load-to-grain angle significantly affected all three embedment properties, confirming the anisotropic embedment behavior of Douglas-fir glulam. Member thickness also showed significant effects on strength and stiffness, although the strength variation was not strictly monotonic. These results are summarized in Table 4.

Table 4. Statistical Analysis Results

Parameter effect	Controlled variables	Response variable	F value	p value	η^2	Statistical interpretation
Bolt diameter	t = 35 mm, θ = 0°	$f_{h,y}$	2.40	0.089	0.204	Not significant
Bolt diameter	t = 35 mm, θ = 0°	$f_{h,u}$	2.32	0.097	0.199	Not significant
Bolt diameter	t = 35 mm, θ = 0°	K_i	44.73	< 0.001	0.827	Significant
Load-to-grain angle	d = 12 mm, t = 30 mm	$f_{h,y}$	28.81	< 0.001	0.767	Significant
Load-to-grain angle	d = 12 mm, t = 30 mm	$f_{h,u}$	9.31	< 0.001	0.515	Significant
Load-to-grain angle	d = 12 mm, t = 30 mm	K_i	51.02	< 0.001	0.854	Significant
Thickness	d = 12 mm, θ = 0°	$f_{h,y}$	71.15	< 0.001	0.871	Significant
Thickness	d = 12 mm, θ = 0°	$f_{h,u}$	31.74	< 0.001	0.751	Significant
Thickness	d = 12 mm, θ = 0°	K_i	10.22	< 0.01	0.493	Significant
Thickness	d = 16 mm, θ = 0°	$f_{h,y}$	16.35	< 0.001	0.609	Significant
Thickness	d = 16 mm, θ = 0°	$f_{h,u}$	13.40	< 0.001	0.561	Significant
Thickness	d = 16 mm, θ = 0°	K_i	19.72	< 0.001	0.653	Significant

Note: The statistical analysis was performed for controlled specimen subsets to isolate the effects of bolt diameter, load-to-grain angle, and member thickness. $f_{h,y}$, $f_{h,u}$, and K_i denote yield embedment strength, ultimate embedment strength, and embedment stiffness, respectively. The significance level was set at $p < 0.05$.

Effect of Bolt Diameters

Figure 6 illustrates the embedment characteristics for different bolt diameters. The initial stiffness of specimens with consistent thickness and identical grain angles (*e.g.*, GL35-8-0 to GL35-16-0) increased significantly with larger bolt diameters. The initial stiffness increased by 70% when the bolt diameter was increased from 8 to 16. This phenomenon is primarily attributable to the increased contact area formed between the larger-diameter fastener and the glued laminated timber substrate.

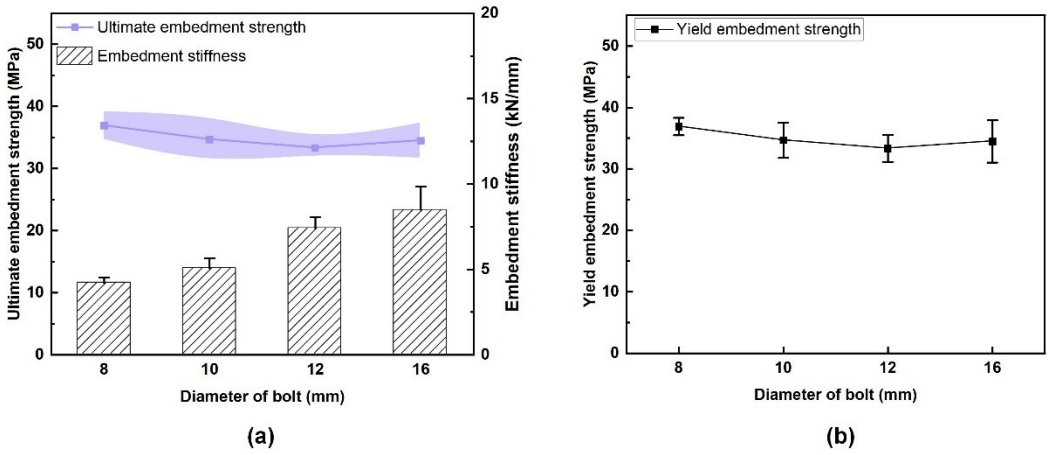


Fig. 6. Embedment characteristics for different bolt diameter: (a) ultimate embedment strengths and embedment stiffness; (b) yield embedment strengths

The greater surface area of the wood fibers allows more of them to participate in load transfer during the elastic stage, thereby reducing localized deformation. This observation is further corroborated by NDS (Wilkinson 1991; AWC-NDS 2024), which states that the embedment stiffness is proportional to the diameter of the fastener, thereby confirming the linear relationship observed in the measured data.

Bolt diameter affected stiffness and normalized embedment strength in different ways. A larger bolt increases the projected bearing area and mobilizes a larger volume of wood fibers during the elastic stage; therefore, the measured embedment stiffness increased markedly with diameter. However, embedment strength is calculated as the load divided by the projected bearing area. This normalized strength does not necessarily increase with diameter, because a larger hole produces a steeper local stress gradient, a wider crushed zone, and more non-uniform contact along the hole boundary. Local yielding may start at the loaded edge before the entire projected area is fully mobilized. Thus, the diameter effect observed here should be interpreted as a stiffness-enhancing effect with only a limited and non-monotonic influence on normalized yield strength. This interpretation is also consistent with the size effect commonly observed in dowel-bearing behavior.

Effect of Load-to-Grain Angles

The angle between the direction of the load and the wood grain has been identified as a crucial factor in determining the embedment strength, stiffness, and failure mechanisms of the wood and wood products (Schweigler *et al.* 2016; Schneid *et al.* 2021). As demonstrated in Fig. 7, when the load direction is parallel to the wood grain (0° angle), specimens consistently demonstrate the highest yield embedment strength and ultimate embedment strength. As the angle increases, the strength values initially decrease and subsequently increase, exhibiting a fluctuating trend. The most significant decline in

strength is observed within the 0° to 30° range, after which a gradual reduction from 30° to 60° is evident, followed by a subsequent recovery between 60° and 90°. This phenomenon has been repeatedly observed in other related studies (Schneid *et al.* 2017; Xu *et al.* 2024). The observed nonlinear variation closely corresponds to the intrinsic anisotropic characteristics of wood. Specifically, mechanical properties such as compressive strength are considerably higher when measured parallel to the grain (longitudinal direction) than when measured perpendicular to the grain (transverse direction). The aforementioned research findings indicate that when analyzing the effects of load size and wood grain orientation on the embedment behavior of timber, it is essential to fully account for the significant variations in characteristics among different tree species and specific load conditions. The angle-dependent variation was further interpreted using the Hankinson-type anisotropic framework, which is widely used to interpolate wood strength between parallel- and perpendicular-to-grain directions. Classical Hankinson behavior reflects the combined contribution of longitudinal and transverse resistance. In the present tests, the lowest strength occurred at an oblique angle rather than under pure perpendicular loading, indicating that the critical state was governed by combined longitudinal compression, transverse tension, and shear around the bolt hole. Therefore, the angle effect cannot be explained by simple monotonic interpolation alone. This finding justifies the use of a modified Hankinson-type model with recalibrated coefficients for Douglas-fir glulam and the present full-hole test configuration.

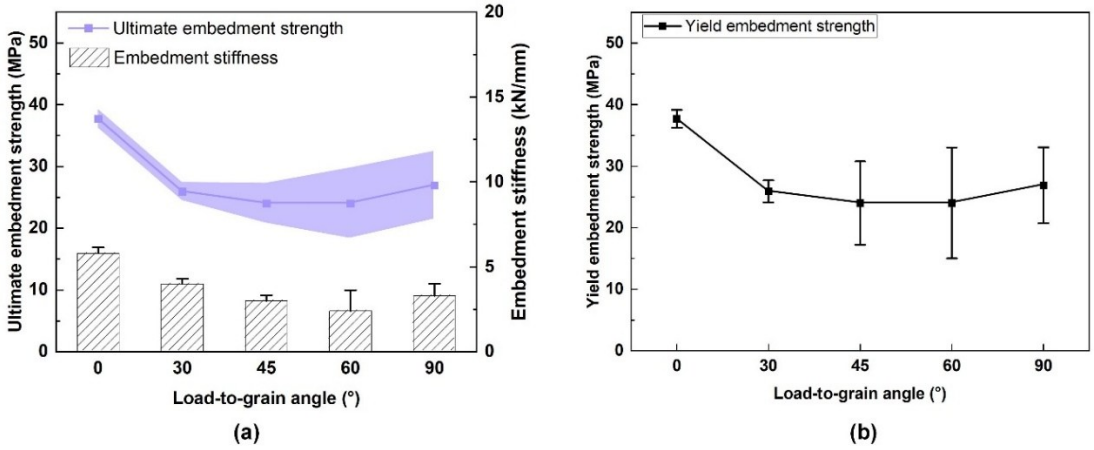


Fig. 7. Embedment characteristics for different load-to-grain angles: (a) ultimate embedment strengths and embedment stiffness; (b) yield embedment strengths

Effect of Thicknesses

Figure 8 presents the variations in embedment characteristics (ultimate embedment strength, yield embedment strength, and embedment stiffness) across different specimen thicknesses (30 mm, 35 mm, 40 mm) for two bolt diameters (M12 and M16). The thickness effect was more evident in embedment stiffness than in embedment strength. For both M12 and M16 bolts, the embedment stiffness increased as the specimen thickness increased from 30 to 40 mm. Specifically, the stiffness increased by 26.9% for the M12 groups and by 48.7% for the M16 groups. This behavior indicates that a thicker glulam member provides a larger bearing volume around the bolt hole, which improves the distribution of local compressive stresses and reduces local deformation during the early loading stage. Therefore, the increase in embedment stiffness can be mainly attributed to a physical bearing-volume effect rather than to random experimental variation. In contrast, the

variation in embedment strength was not strictly monotonic over the 30–35–40 mm thickness range. Although the 40 mm specimens generally showed higher yield and ultimate embedment strengths, the 35 mm groups did not always exceed the 30 mm groups. This non-monotonic strength trend suggests that the thickness effect on strength was coupled with local material heterogeneity, including lamina-level density variation, glue-line distribution, and local defects around the bolt-bearing zone. As a result, member thickness should be regarded as an influential factor for embedment performance, particularly for stiffness, but its effect on strength should not be interpreted as a simple linear increase with thickness. The present comparison is limited to the parallel-to-grain thickness subsets tested in this study; therefore, additional angle–thickness combinations are required to further clarify the coupled influence of member thickness and load-to-grain angle. Compared with the results reported by Zhang *et al.* (2025), the present stiffness trend differs in magnitude and sensitivity. This discrepancy may be associated with differences in test configuration, bolt–hole clearance, and the examined diameter-to-thickness ratio range. These differences further indicate that thickness-dependent embedment behavior is configuration-sensitive and should be interpreted within the specific boundary conditions of the test program.

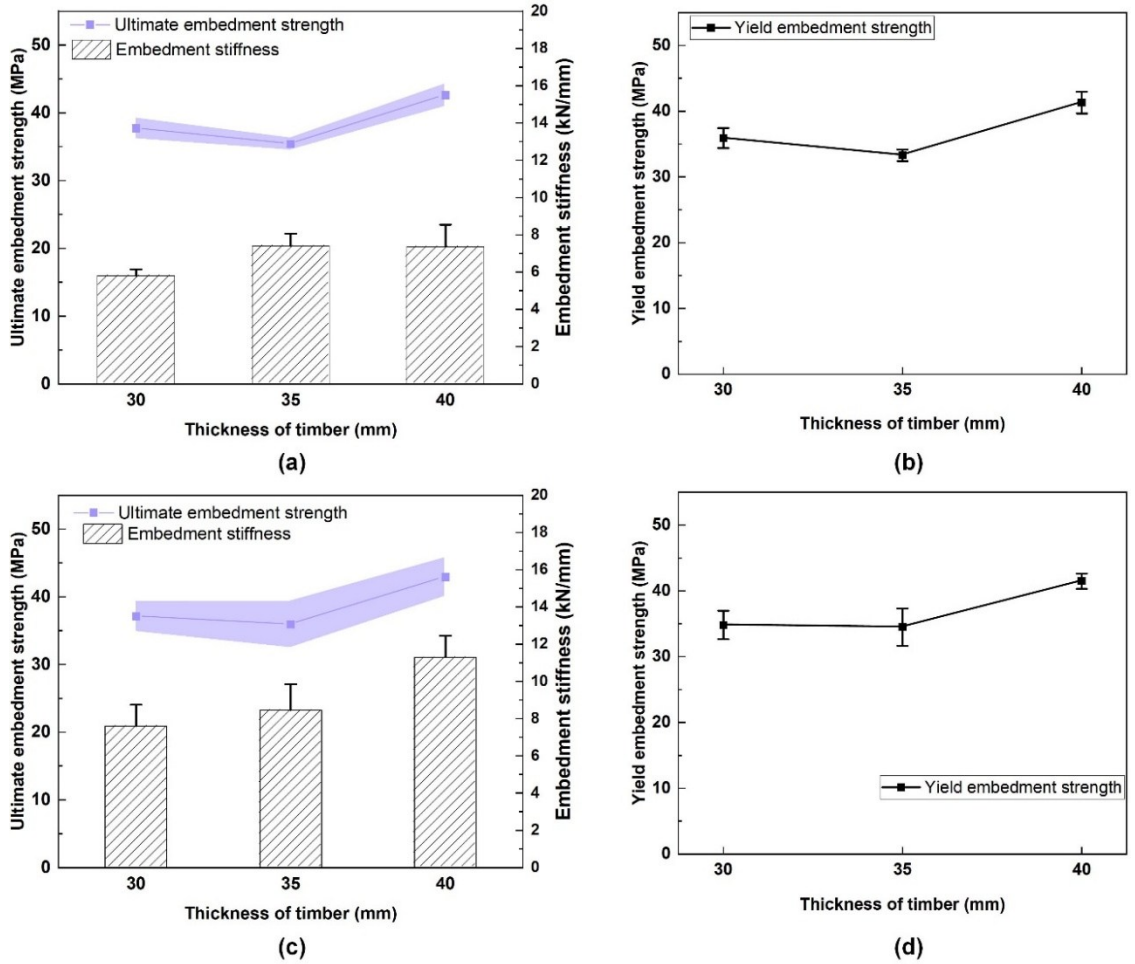


Fig. 8. Embedment characteristics for different timber thickness: (a) ultimate embedment strengths and embedment stiffness for 12 mm diameter; (b) yield embedment strengths for 12 mm diameter; (c) ultimate embedment strengths and embedment stiffness for 16 mm diameter; (d) yield embedment strengths for 16 mm diameter

Prediction of Embedment Strength

To evaluate the suitability of existing international design standards for predicting the embedment strength of glulam, this study compared the experimental results with predictions derived from two widely used design models: Eurocode 5 (EN 1995-1 2025) and the NDS (AWC-NDS 2024). Since all these models were originally calibrated based on data from solid sawn timber, it is essential to assess their accuracy when applied to glulam, which has a distinct layered structure and anisotropic material behavior. This validation is crucial for ensuring the structural reliability and safety of glulam components in engineering applications.

The EC5 model predicts the characteristic embedment strength of timber for dowel-type fasteners using the density and diameter of fasteners as the core input parameter. It provides a single formula for embedment strength that implicitly accounts for loading direction through adjustment factors. The formula is shown in Eq. 3,

$$\begin{cases} f_{\mathrm{h,k}} = 0.082\ (1-0.01\,d)\rho_{\mathrm{k}} & d \le 8 \text{ mm} \\ f_{\mathrm{h,k}} = \dfrac{0.082\ (1-0.01\,d)\rho_{\mathrm{k}}}{k_{90}\sin^2\theta + \cos^2\theta} & d > 8 \text{ mm} \end{cases} \tag{3}$$

where ρ_{k} is the characteristic density, and $k_{90} = 0.9 + 0.015d$.

The NDS model adopts a more empirical approach, incorporating both timber density and fastener diameter as predictive variables. The model accounts for the influence of loading direction relative to the wood grain, with separate formulations for parallel-to-grain and perpendicular-to-grain loading. The base formula for the nominal embedment is shown in Eq. 4,

$$f_{\mathrm{h,k}} = \frac{f_{e\parallel} f_{e\perp}}{f_{e\parallel}\sin^2\theta + f_{e\perp}\cos^2\theta} \tag{4}$$

where $f_{e\parallel} = 0.07725\rho$, $f_{e\perp} = 0.0095\rho^{1.45}d^{-0.5}$.

The comparison between the predicted embedment strength values derived from the EC5 and NDS models and the corresponding actual experimental values is presented in Fig. 9 (a) and (b), respectively. The deviations of EC5 and NDS can be attributed to both calibration background and model structure. The EC5 expression is primarily governed by density and fastener diameter and was originally developed for general timber design rather than for the specific layered architecture of Douglas-fir glulam. The NDS formulation separates parallel- and perpendicular-to-grain embedment properties and introduces empirical angle dependence, but it still does not explicitly consider lamination arrangement, glue-line effects, hole clearance, or the mixed compression–shear–tension state generated under oblique bearing. Consequently, both standards may provide reasonable estimates for some parallel-to-grain cases but show larger deviations for off-axis loading, where splitting and shear-related mechanisms become more important. To enhance the applicability of the prediction model, this study adopted the benchmark model provided by the Hankinson formula (Bodig *et al.* 1982; AWC-NDS 2024) as its foundation. The modified prediction model was ultimately developed through systematic parameter adjustments and structural optimization, as follows,

$$f_{h,y} = \frac{f_{e\parallel} f_{e\perp}}{f_{e\parallel} \sin^{1.15}\theta + f_{e\perp} \cos^{0.6}\theta} \quad (5)$$

where $f_{e\parallel} = 0.075\rho$, $f_{e\perp} = 1.5\rho^{0.88} d^{-1.1}$.

The coefficients of the modified Hankinson-type model were obtained by nonlinear least-squares regression using the present test data, with the objective function defined as the minimization of the squared relative error between predicted and measured yield embedment strengths. The coefficient signs and exponents were constrained to remain mechanically meaningful: density-related terms were required to increase resistance, whereas diameter-related and angle-related terms were allowed to reflect size effect and anisotropic stress redistribution. Model performance was evaluated using the mean prediction-to-test ratio, coefficient of variation of the prediction ratio, mean absolute percentage error, root-mean-square error, and coefficient of determination. In addition to the present dataset, published embedment data for dowel-type fasteners in timber and engineered wood products (Sawata *et al.* 2002; Santos *et al.* 2010; Schneid *et al.* 2017; Ottenhaus *et al.* 2022; Xu *et al.* 2022; Xu *et al.* 2024) were used as an external comparison to assess whether the model retained reasonable predictive capability beyond the calibration set. The model is therefore presented as a calibrated design-oriented expression for the tested material and configuration, not as a universal equation for all glulam products.

Figure 9(c) provides a clear visual representation of the comparison between the values predicted by the modified model and the corresponding experimentally measured values. The results suggest that the present glulam follows the general Hankinson-type anisotropy pattern, but the density and diameter exponents require recalibration when moving from sawn timber to glulam.

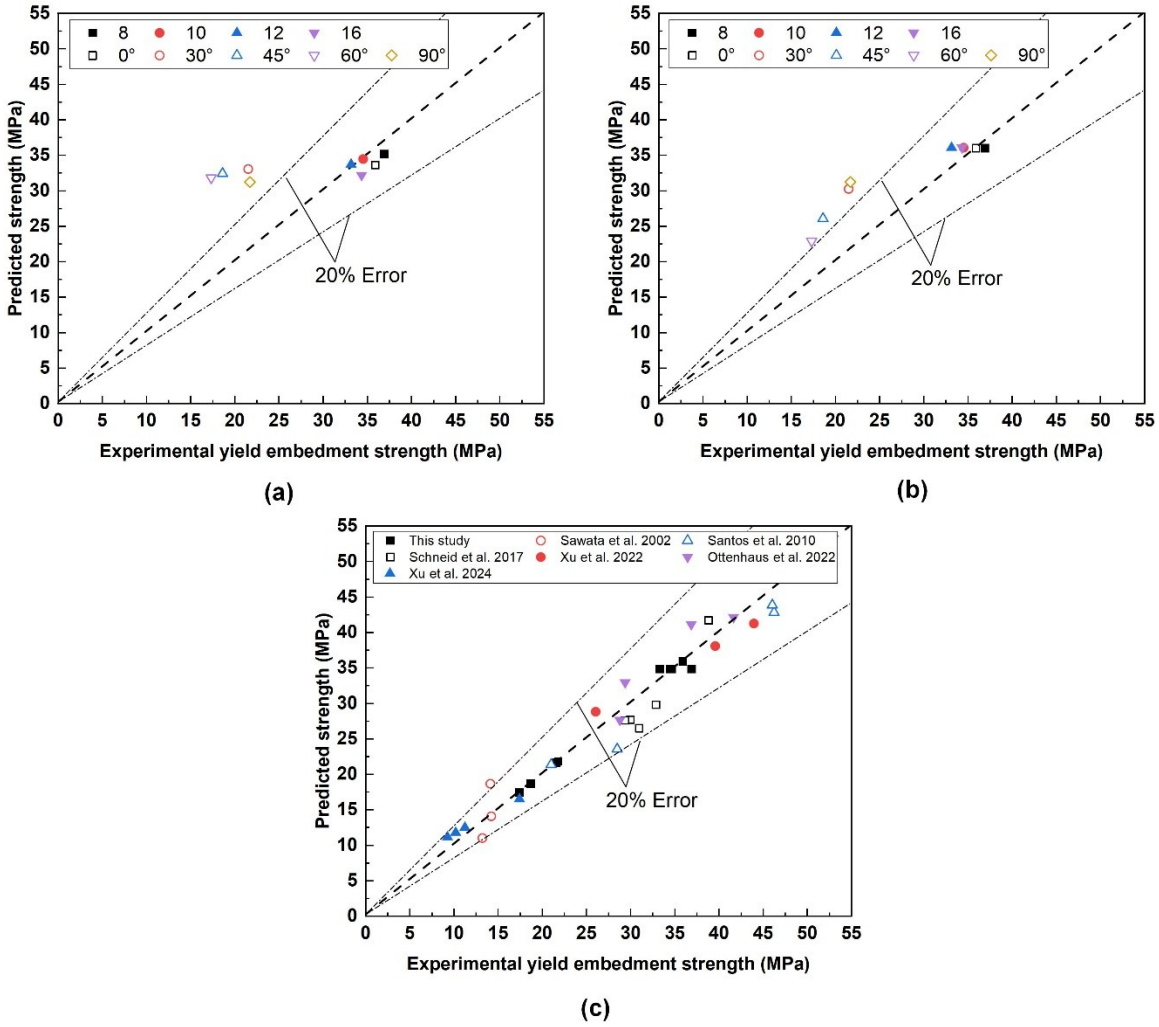


Fig. 9. Comparison of yield embedment strength measured in tests with model-predicted values: (a) EC5; (b) NDS; (c) modified model

Prediction of Embedment Stiffness

Glulam embedment stiffness is not addressed by international design standards, which lack unified and explicit prediction models for embedment stiffness. Eurocode 5 (EN 1995-1 2025) only defines embedment stiffness as the slope between 0.1 F_{max} and 0.4 F_{max} in the load-displacement curve but does not provide a quantitative prediction formula, relying instead on experimental testing for specific configurations. The American NDS 2024 (AWC-NDS 2024) specification briefly correlates stiffness with timber density and fastener diameter but adopts a simplified linear relationship that ignores the combined effects of specimen thickness and load-to-grain angle, leading to significant prediction deviations in practical applications. The modified stiffness prediction model based on the Hankinson formula is shown in Eq. 6,

$$K_{\theta} = \frac{0.05\rho^{0.38} d^{1.1}}{2\sin^{1.6}\theta + 1.2\cos^{0.1}\theta} \quad (6)$$

where K_{θ} means the initial embedment stiffness of the timber under load at any angle.

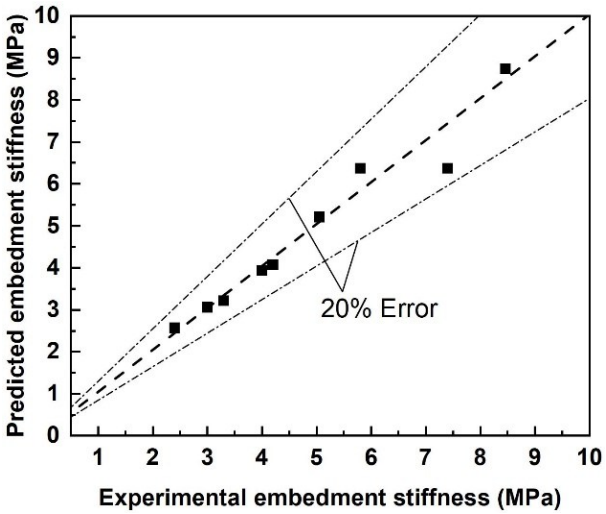


Fig. 10. Comparison of embedment stiffness measured in tests with model-predicted values

Figure 10 compares the experimentally measured embedment stiffness with the values predicted by the theoretical model. Although the equation captures the main diameter- and angle-related tendencies observed in the present data, it does not explicitly include member thickness, hole clearance, lamination layout, moisture condition, or possible interaction terms. A full multivariable stiffness model was not calibrated because the experimental matrix was not fully factorial for all combinations of diameter, angle, and thickness, and adding additional terms would risk overfitting. Therefore, Eq. 6 is recommended only for preliminary comparison within the tested range of Douglas-fir glulam, bolt diameters, and clearance conditions.

All tests were conducted under laboratory conditions using specimens conditioned to approximately 12% moisture content. The results therefore represent short-term embedment behavior under controlled moisture and temperature conditions. In practical structures, moisture variation, wetting–drying cycles, temperature changes, and long-term loading may alter the stiffness, crushing resistance, dimensional stability, and glue-line behavior of glulam. These environmental effects were outside the scope of the present experimental program and should be considered before applying the proposed equations to other service classes or exposure conditions.

CONCLUSIONS

1. The experimental results demonstrate that the embedment behavior of Douglas-fir glulam with low-to-medium diameter bolts is governed primarily by load-to-grain angle and member thickness, whereas bolt diameter mainly affects embedment stiffness rather than strength. Increasing the bolt diameter from M8 to M16 markedly increased the initial embedment stiffness, but the corresponding changes in yield and ultimate embedment strengths were relatively limited. This indicates that, for the tested diameter range and 1 mm hole clearance, bolt diameter should be considered mainly as a stiffness-related design parameter rather than as a direct strength-enhancement factor.
2. The load-to-grain angle had the most pronounced influence on embedment strength, stiffness, and failure mode. The strength decreased substantially from parallel-to-grain

loading to oblique loading and then partially recovered at 90°, confirming that the angle effect cannot be represented by a simple linear reduction. For engineering design, this result suggests that off-axis loading in bolted glulam connections should be explicitly considered, particularly when bolts are used in beam-to-column, splice, or inclined-force transfer zones. A Hankinson-type formulation is more appropriate than a single parallel- or perpendicular-to-grain value for describing the anisotropic embedment resistance of glulam.

3. Member thickness improved the overall embedment response, especially the embedment stiffness, because thicker specimens provided a larger bearing volume and more effective stress redistribution around the bolt hole. However, the strength increase was not strictly monotonic over the 30–35–40 mm thickness range, indicating that thickness effects may be coupled with local lamination characteristics, glue-line distribution, and material heterogeneity. Therefore, thickness should be included in the interpretation of embedment performance, but its effect on strength should not be simplified as a purely linear increase.
4. The comparison with Eurocode 5 and NDS showed that design equations calibrated mainly for sawn timber may produce noticeable deviations when applied to Douglas-fir glulam, especially under off-axis loading. The modified Hankinson-type model provided closer agreement with the measured yield embedment strengths and may serve as a useful supplementary basis for the design assessment of low-to-medium diameter bolted glulam connections. Nevertheless, the proposed model should be regarded as applicable only within the tested material, bolt diameter, thickness, and hole-clearance ranges. Further validation is required before it can be generalized to other species, glulam grades, moisture conditions, long-term loading conditions, or different bolt-hole clearances.
5. From a practical perspective, the present results indicate that glulam connection design should not rely solely on sawn-timber-based embedment equations. Future standard development could benefit from incorporating product-specific calibration factors for glulam, angle-dependent embedment resistance, and stiffness-related parameters for serviceability assessment. These additions would improve the reliability of bolted glulam connection design, particularly for engineered timber structures where connection stiffness and anisotropic load transfer strongly influence global structural performance.

ACKNOWLEDGMENTS

The authors greatly appreciate the financial support from the Heilongjiang Provincial Key R&D Program Guidance Category Project (Grant No. GZ2024011).

Conflict of Interest

The authors declare that they have no known competing financial interests or personal relationships that could have appeared to influence the work reported in this paper.

REFERENCES CITED

ASTM D 5764 (2018). "Standard test method for evaluating dowel-bearing strength of wood and wood-based products," American Society of Testing Materials (ASTM), Philadelphia, USA.

Aquino, C. D., Rodrigues, L. G., Schweigler, M., Kržan, M., Li, Z., and Branco, J. M. (2024). "Influence of test methodology on the characterization of the parallel-to-grain timber embedment strength and foundation modulus of dowels," *Wood Mater Sci Eng* 20(1), 94-106. https://doi.org/10.1080/17480272.2024.2328088

AWC-NDS (2024). "National design specification (NDS) for wood construction," American Wood Council, Leesburg, VA, USA.

Bodig, J., and Jayne, B. A. (1982). *Mechanics of Wood and Wood Composites*, Van Nostrand Reinhold Company, New York.

Cabrero, J. M., Honfi, D., Jockwer, R., and Yurrita, M. (2019). "A probabilistic study of brittle failure in dowel-type timber connections with steel plates loaded parallel to the grain," *Wood Mater Sci Eng* 14(5), 298-311. https://doi.org/10.1080/17480272.2019.1645206

Cabrera, G., Moltini, G., and Baño, V. (2022). "Embedment strength of low- and medium-density hardwood species from Spain," *Forests* 13(8), article 1154. https://doi.org/10.3390/f13081154

EN 383 (2007). "Timber structures-test methods-determination of embedment strength and foundation values for dowel type fasteners," European Committee for Standardization (CEN), Brussels, Belgium.

EN 1995-1 (2025). "Eurocode 5: Design of timber structures — Part 1-1: General rules and rules for buildings," European Committee for Standardization, Brussels, Belgium.

Franke, S., and Magnière, N. (2014). "Discussion of testing and evaluation methods for the embedment behavior of connections," in: *Proceedings of the International Network on Timber Engineering Research*, Bath, UK.

GB/T 26899 (2022). "Structural glued laminated timber," China Architecture and Building Press, Beijing, China.

GB/T 50329 (2012). "Standard for test methods of timber structures," China Architecture and Building Press, Beijing, China.

Hager, K. (1930). "Der Lochleibungsdruck bei Holzverbindungen," *Der Bauingenieur* 11(50), 865-866.

Hirai, T. (1989). "Rational testing methods for determination of basic lateral resistance of bolted wood-joints," *Research Bulletins of the College Experiment Forests Hokkaido University* 46.

Issa, C. A., and Kmeid, Z. (2005). "Advanced wood engineering: Glulam beams," *Constr. Build. Mater* 19(2), 99-106. https://doi.org/10.1016/j.conbuildmat.2004.05.013

Jeong, G. Y., Kong, J. H., Lee, S. J., and Pang, S.-J. (2018). "Comparisons of bearing properties for various oriented glulam using digital image correlation," *J. Wood Sci.* 64(3), 237-245. https://doi.org/10.1007/s10086-018-1700-5

Johansen, K. W. (1949). "Theory of timber connections," *International Assoc. of Bridge Structural Engineering Publication* 9, 249-262.

Mack, J. J. (1981). *The strength of Bolted Joints in Australian Timbers*, CSIRO Division of Building Research Technical Paper (Second Series), Melbourne, Australia.

Ottenhaus, L.-M., Jockwer, R., van Drimmelen, D., and Crews, K. (2021). "Designing timber connections for ductility–A review and discussion," *Constr. Build. Mater* 304, article 124621. https://doi.org/10.1016/j.conbuildmat.2021.124621

Ottenhaus, L.-M., Li, Z., and Crews, K. (2022). "Half hole and full hole dowel embedment Strength: A review of international developments and recommendations for Australian softwoods," *Constr. Build. Mater* 344. https://doi.org/10.1016/j.conbuildmat.2022.128130

Sandhaas, C., Ravenshorst, G. J. P., Blass, H. J., and van de Kuilen, J. W. G. (2013). "Embedment tests parallel-to-grain and ductility aspects using various wood species," *Eur. J. Wood Wood Prod* 71(5), 599-608. https://doi.org/10.1007/s00107-013-0718-z

Santos, C. L., De Jesus, A. M. P., Morais, J. J. L., and Lousada, J. L. P. C. (2010). "A comparison between the EN 383 and ASTM D5764 test methods for dowel-bearing strength assessment of wood: Experimental and numerical investigations," *Strain* 46(2), 159-174. https://doi.org/10.1111/j.1475-1305.2008.00570.x

Sawata, K., and Yasumura, M. (2002). "Determination of embedding strength of wood for dowel-type fasteners," *J. Wood Sci.* 48(2), 138-146. https://doi.org/10.1007/BF00767291

Schneid, E., and de Moraes, P. D. (2017). "Grain angle and temperature effect on embedding strength," *Constr. Build. Mater* 150, 442-449. https://doi.org/10.1016/j.conbuildmat.2017.06.015

Schneid, E., and Dias de Moraes, P. (2021). "Modification factors of the embedding strength dependent on the temperature and load-to-grain angle for two wood species planted in Brazil," *Constr. Build. Mater* 271, article 121503. https://doi.org/10.1016/j.conbuildmat.2020.121503

Schweigler, M., Bader, T. K., Hochreiner, G., Unger, G., and Eberhardsteiner, J. (2016). "Load-to-grain angle dependence of the embedment behavior of dowel-type fasteners in laminated veneer lumber," *Constr. Build. Mater* 126, 1020-1033. https://doi.org/10.1016/j.conbuildmat.2016.09.051

Smith, I., and Foliente, G. (2002). "Load and resistance factor design of timber joints: International practice and future direction," *J. Struct. Eng.* 128(1), 48-59. https://doi.org/10.1061/(ASCE)0733-9445(2002)128:1(48)

Tuhkanen, E., Mölder, J., and Schickhofer, G. (2018). "Influence of number of layers on embedment strength of dowel-type connections for glulam and cross-laminated timber," *Eng. Struct.* 176, 361-368. https://doi.org/10.1016/j.engstruct.2018.09.005

Wang, Y., Bao, Y., Aquino, C. D., Schweigler, M., Wang, T., and Crocetti, R. (2025). "Compare EN 383 and ASTM D5764 on the embedment properties of plywood: Influence of test setups, specimen geometry, and loading procedures," *Constr. Build. Mater* 490, article 142377. https://doi.org/10.1016/j.conbuildmat.2025.142377

Wilkinson, T. L. (1991). *Dowel Bearing Strength* (Vol. 505), U.S. Department of Agriculture, Forest Service, Forest Products Laboratory, Washington, USA.

Xu, B.-H., Guo, H.-F., Li, X.-L., Zhao, Y.-H., and Zhang, B. (2024). "Embedment strength and foundation modulus at an angle to the grain for fully threaded bolts," *Wood Mater Sci Eng* 19(5), 1117-1129. https://doi.org/10.1080/17480272.2024.2304138

Xu, B.-H., Jing, C.-K., and Bouchaïr, A. (2021). "Experimental analysis of the influence of the fastener type on the embedment strength parallel to the grain in glued laminated timber," *J. Mater. Civ. Eng* 33(2), 06020023. https://doi.org/10.1061/(ASCE)MT.1943-5533.000359

Xu, B.-H., Lin, J.-B., Zhao, Y.-H., and Bouchaïr, A. (2022). "Embedment behavior of fully threaded bolts in glued laminated timber," *Eur. J. Wood Wood Prod* 81(2), 369-386. https://doi.org/10.1007/s00107-022-01901-8

Yurrita, M., Cabrero, J. M., and Moreno-Zapata, E. (2021). "Brittle failure in the parallel-to-grain direction of timber connections with small diameter dowel-type fasteners: A new design model for plug shear," *Eng. Struct*. 241, 112450. https://doi.org/10.1016/j.engstruct.2021.112450

Zhang, C., Yang, H., Tian, Y., Chen, W., Tao, H., and Shi, B. (2025). "Embedment stiffness prediction of smooth dowel-type fasteners in glued-laminated timber," *Wood Mater Sci Eng*, 1-13. https://doi.org/10.1080/17480272.2025.2595067

Article submitted: April 23, 2026; Peer review completed: May 25, 2026; Revised version received: May 26, 2026; Accepted: May 28, 2026; Published: June 9, 2026.
DOI: 10.15376/biores.21.3.6781-6800